East European Journal of Physics. 4. 469-483 (2025)
DOI:10.26565/2312-4334-2025-4-48 ISSN 2312-4334

DFT-BASED STUDY OF TlX AND BX (X= N, P, As) COMPOUNDS: A COMPARATIVE INSIGHT INTO STRUCTURAL, ELECTRONIC, AND OPTICAL BEHAVIOR

Abed Zoulikha*, Lachabi Abdelhadi, Abdelali Laid
Applied Materials Laboratory, Research Center, Sidi Bel Abbes University, 22000, Algeria
**Corresponding Author E-mail: zoulikhaabed3@gmail.com*
E-mail co-authors: lachebia@yahoo.fr; laidabdelali@gmail.com
Received July 28, 2025; revised October 17, 2025; accepted November 1, 2025

This work presents a detailed theoretical investigation of the structural, electronic, and optical properties of thallium-based (TlX) and boron-based (BX) compounds, where X = N, P, As, within the zinc-blende crystal structure. First-principles calculations were performed using density functional theory (DFT) within the generalized gradient approximation (GGA). The obtained results reveal that Tl-based compounds exhibit lower total energies compared to BX compounds, indicating higher structural stability. In terms of electronic behavior, BX compounds maintain their semiconducting nature. In contrast, TlX compounds show metallic or near-metallic characteristics due to the absence of an energy gap at the Fermi level. Furthermore, optical investigations demonstrate that TlX compounds possess higher static refractive indices and stronger absorption features in the low-energy region. These findings highlight the potential of Tl-based compounds for future applications in optoelectronic and photonic devices. Overall, this comparative study provides valuable insights for the design of advanced materials for electronic and energy-related technologies.
Keywords: *Thallium compounds; Boron compounds; First-principles calculations; Density functional theory (DFT); Electronic properties; Band structure; Semiconductors; TlX; BX*
PACS: 84.60.Jt;78.20.Bh;89.30.Cc;42.60.Lh

1. INTRODUCTION

In recent years, the investigation of the structural, electronic, and optical properties of III-V semiconductors has attracted considerable attention due to their potential applications in advanced electronic and optoelectronic devices. Among these compounds, boron-based (B-V) and thallium-based (Tl-V) materials have emerged as promising candidates thanks to their unique electronic band structures, wide-ranging energy gaps, and favorable optical characteristics. These compounds have been extensively studied through both experimental techniques and first-principles calculations, especially those based on density functional theory (DFT), which remains a reliable and widely used approach for predicting the fundamental properties of materials at the atomic scale. It is evident that there has been a significant interest in using first-principles calculations [2, 11, 12, 14], including density functional theory (DFT) [9, 13], to investigate the structural and electronic properties of III-V semiconductors and superlattice structures. The physical properties of B-V and Tl-V compounds have been the subject of extensive theoretical and experimental research. In this context, several relevant studies can be mentioned, such as the work of *Akshay* [1], who focused on the structural and electronic properties of BN compounds, as well as the theoretical studies of *Yousra Megdoud* [6], which were dedicated to the structural and electronic investigation of BX compounds where X = N, P, As. Furthermore, *Nawel Saidi* [3] has conducted an in-depth study on Tl-V compounds, emphasizing the influence of structural aspects on their electronic behavior. Within this scientific context, the present work is devoted to a comprehensive first-principles investigation of the structural, electronic, and optical properties of boron-based (BX with X = N, P, As) and thallium-based (TlX with X = N, P, As) compounds in the zinc blende phase. In all calculations carried out in this study, the density functional theory (DFT) framework has been adopted, employing the generalized gradient approximation (GGA) to describe the exchange-correlation effects accurately.

The aim is to provide a systematic and comprehensive comparison between thallium-based (TlX) and boron-based (BX) compounds, where X = N, P, As, focusing on their structural stability, electronic band structures, density of states, and optical response. The novelty of this study lies in its unified theoretical approach, as most previous investigations have considered each compound separately, without drawing a direct comparison between these two families.

By adopting this comparative perspective, the present work seeks to highlight both the key differences and possible similarities, thereby evaluating their suitability for future optoelectronic applications.

2. METHOD

The theoretical calculations in this study were performed using the WIEN2k Software package [8], which empioys the (FP-LAPW) technique under the theoretical framework of density functional theory (DFT). This method is considered one of the most accurate for studying the structural and electronic properties of crystalline solids, as it imposes no shape approximation on the potential or electron density, making it particularly well-suited for systems containing heavy atoms such as thallium. The generalized Gradient Approximation (GGA) in the Perdew-Burke-Erzerhof (PBW) form was adopted to describe the exchange-correlation interactions between electrons [5]. This functional has proven effective in accurately modeling the ground state properties of semiconductors and complexes compounds.

Cite as: A. Zoulikha, L. Abdelhadi, A. Laid, East Eur. J. Phys. 4, 469 (2025), https://doi.org/10.26565/2312-4334-2025-4-48

(i) Crystal Structure setup: the made compounds TlX and BX were modeled in the zinc blend (ZB) structure, which belongs to the F-43m (No.216) space group. This cubic arrangement is widely observed in III-V semiconductors [10]. In this structure, the thallium and boron atoms occupy the positions of a face-centered cubic (FCC) lattice, while the group V atoms (N, As, P) are shifted by (0.25, 0.25, 0.25) within the unit cell, thus occupying the tetrahedral sites of the FCC lattice.

(ii) ***Numerical parameters:*** To avoid overlap between atomic spheres, the muffin-tin radii ($_{RMT}$) were carefully chosen for each atom, the product $_{RMT}$ x $_{Kmaa}$ = 7.0. The Brillouin Zone (BZ) was sampled using a Monkhorst-Pack k-point mesh [10] of at least 11x11x11 to guarantee convergence of total energy and electronic properties.
A total of 56 k-points were employed for the integration over the irreducible part of the Brillouin zone. The convergence of the total energy with respect to ensure the accuracy of the calculations.

(iii) ***Structural optimization:*** The optimal lattice constant was obtained by evaluating the total energy as a function of the unit cell volume. The resulting energy-volume data were then fitted using the *Murnaghan equation of state* [7] to identify the minimum energy and the corresponding equilibrium structural parameters. All subsequent calculations were carried out using this optimized geometry.

$$E(V) - E(V_0) = \frac{B_0 V}{B_0'}\left[\frac{(V_0|V)^{B_0'}}{B_0'-1} + 1\right] - \frac{B_0 V_0}{B_0'-1}, \quad (1)$$

$$B_0 = V\frac{\partial^2 E}{\partial V^2} = \frac{4}{9a}\frac{\partial^2 E}{\partial a^2} \quad (2)$$

Where B_0 is the bulk modulus given by the relation (1-b) at zero pressure (P=0), V_0 is the equilibrium volume, E (V_0) is the energy corresponding to equilibrium volume, B_0' is the pressure derivative of the bulk modulus at P=0 and, a is lattice constant.

(iv) Electronic Properties: with the optimized structure; self-consistent field (SCF) calculations were performed to obtain the band structure along high-symmetry directions in the Brillouin zone, as well as the total and partial density of states (DOS). These results provided insights into the nature of the band gap (direct or indirect), its magnitude, and the orbital contributions from different atomic states near the valence and conduction bands [4].

(v) Optical Properties: the optical properties were evaluated using the optics module of WIEN2K, which computes the complex dielectric function based on the electronic structure. From the real and imaginary parts of the dielectric function, various optical constants were extracted, including the refractive index, absorption coefficient, reflectivity, and energy loss function [4]. These quantities are essential for materials in optoelectronic and photonic application.

In this work, different muffin-tin radii were chosen for each atom in order to improve the accuracy of the calculations within the WIEN2K framework [8]. These values were selected to avoid overlap between spheres and to ensure numerical stability during the DFT simulation. The Table 1 summarizes the selected muffin-tin radii for each atomic species, along with their corresponding electronic configuration to properly define valence states.

Table 1. Atomic muffin-tin radii and corresponding electronic configurations

Element	*Rmt (a.u.)*	*Z*	*Full Electronic Configuration*	*Valence Electrons Treated in DFT*
Tl	2.50	81	[Xe] $4f^{14}$ $5d^{10}$ $6s^2$ $6p^1$	$5d^{10}$ $6s^2$ $6p^1$
B	1.60	5	$1s^2$ $2s^2$ $2p^1$	$2s^2$ $2p^1$
N	1.55	7	$1s^2$ $2s^2$ $2p^3$	$2s^2$ $2p^3$
P	1.85	15	[Ne] $3s^2$ $3p^3$	$3s^2$ $3p^3$
As	1.90	33	[Ar] $3d^{10}$ $4s^2$ $4p^3$	$3d^{10}$ $4s^2$ $4p^3$

3. ANALYSIS AND INTERPRETATION OF RESULTS

3.1. Structural parameters

Figure 1 illustrates the crystal structures of the TlX and BX compounds where X = N, P, As. All these compounds crystallize in the zinc-blende (B3) structure. This structure belongs to the face-centered cubic (FCC) system and consists of two interpenetrating cubic sublattices displaced by one quarter of the body diagonal of the unit cell.

In the primitive cell, the B and X atoms in the BX compounds, as well as the Tl and X atoms in the TlX compounds occupy the Cartesian positions (0, 0, 0) and (a/4, a/4, a/4) respectively, where a denotes the conventional cubic lattice parameter. Each unit cell contains four boron atoms and each boron atom is surrounded by four X atoms arranged in a tetrahedral configuration. Thus, the unit cell contains sixteen X atoms distributed around the boron atoms.

A similar arrangement is observed for the TlX compounds where each thallium atom is coordinated to four X atoms in the same tetrahedral geometry. This atomic arrangement gives these compounds a high degree of crystalline symmetry belonging to the space group (F-43m) which is characteristic of the zinc-blende structure.

The lattice constant (a), equilibrium volume (V_0), bulk modulus (B_0), its pressure derivative (B_0'), and the total ground-state energy (E) were calculated using density functional theory (DFT) within the generalized gradient approximation (GGA), for BX and TlX compounds (X = N, P, As) in the zinc-blende (ZB) structure. The results are summarized in the Table 2 and 3.

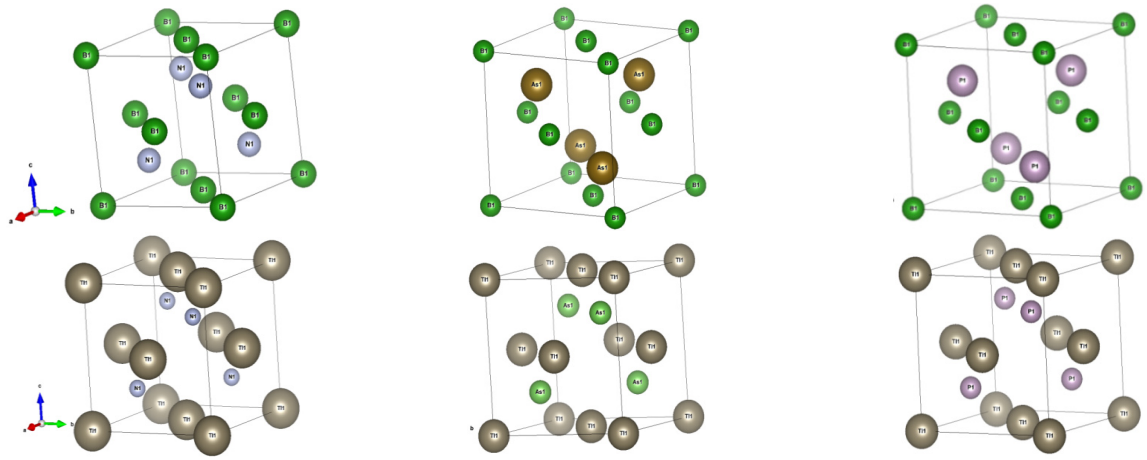

Figure 1. Optimized crystal structures of BX and of TlX compounds obtained from our calculations using the GGA approximation

Table 2. Values of lattice parameter a (Å), bulk modulus (B_0), pressure derivative of the bulk modulus (B0') equilibrium volume (V_0), and total energy of TlX compounds:

		a (Bohr)	a (Å)	B_0 (GPa)	B_0'	V_0 (Ry)	E (Ry)
TlN	Calculations	9.9803	5.2814	89.3550	4.9537	248.5287	-40687.222951
	Other calculatios	- -	5.2723 [15] 5.297 [16] 5.267 [20]	94.06 [15] 89.723 [16] 101.5 [20]	4.3038 [15] 5.026 [16] 3.9 [20]	- -	-40687.232557 [15] -
TlP	calculations	11.5659	6.1208	45.9402	4.9292	386.869	-41262.006475
	Other calculatios	- -	6.135 [16] 5.96 [19] 6.124 [3]	44.981 [16] 57 [19] 46.75 [3]	4.8771 [16] - -	- - -	- - -
TlAs	calculations	12.0088	6.3548	38.1483	4.8986	432.9475	-45099.985275
	Other calculatios	- -	6.374 [16] 6.170 [21]	37.196 [16] 50.2 [21]	4.910 [16] -	- -	- -

Table 3. Values of lattice parameter a (Å), bulk modulus (B_0), pressure derivative of the bulk modulus (B0') equilibrium volume (V_0) and total energy of BX compounds

		a (bohr)	a (Å)	B_0 (GPa)	B_0'	V_0 (Ry)	E (Ry)
BN	calculations	6.855	3.6280	373.1226	3.7538	80.5613	-159.394567
	experimental		3.615 [22]	369 [22]	4 [22]	-	-
	Other calculatios	- -	3.530 [17] 3.606 [18]	417.44 [17] 367 [18]	3.78 [17] -	- -	- -
BP	calculations	8.5986	4.5502	161.5866	3.6769	158.9336	-733.960301
	experimental		4.538[23]				
	Other calculatios	-	4.558[18] 4.425[17]	166[18] 182.81[17]	- 3.77[17]	- -	- -
BAs	calculations	9.0947	4.8127	130.9268	4.0777	188.0645	-4571.898798
	experimental		4.777 [24]	-	-	-	-
	Other calculatios	- -	4.668[17] 4.777 [18]	154.30[17] 145 [18]	3.87[17] -	- -	- -

The obtained data, illustrated in Figures 2 and 3 and supported by the results shown in Tables 2 and 3, clearly demonstrate a significant contrast in the structural stability and total energy between thallium-based compounds (TlX) and boron-based compounds (BX), where X = N, P, As. Thallium compounds exhibit much more negative total energies, which indicates higher thermodynamic and dynamical stability. For instance, the total energy of TlN is about −40637.22 Ry, while that of TlP and TlAs reaches −43461.54 Ry and −45099.98 Ry respectively, compared to the boron-based compounds BN (−159.39 Ry), BP (−4414.99 Ry), and BAs (−4571.89 Ry), confirming the superior energetic stability of Tl-based materials.

Regarding mechanical properties, the calculated equilibrium volume (Vo) and bulk modulus (Bo) reveal fundamental structural differences between the two families. TlX compounds are characterized by larger equilibrium volumes and lower bulk moduli, indicating relatively softer crystal structures. For example, TlP has a Vo of 271.37 a.u³ and Bo of 33.14 GPa, while TlAs displays an even larger Vo (296.76 a.u³) and a lower Bo (28.21 GPa). In contrast, BX compounds are more compact and mechanically robust, particularly BN, which shows the smallest Vo (80.56 a.u³) and the highest Bo (373.12 GPa), pointing to high mechanical hardness and strong covalent bonding.

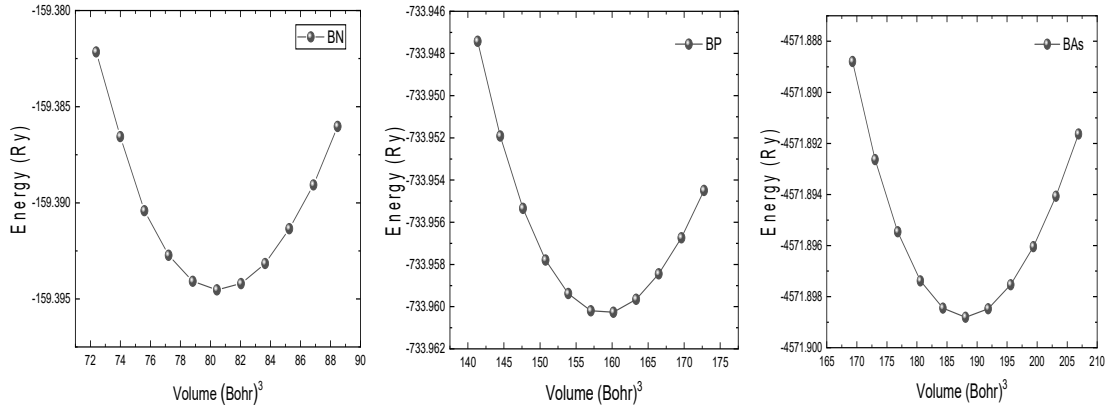

Figure 2. Variation of total energy as a function of atomic volume for BX compounds in the zinc blend structure

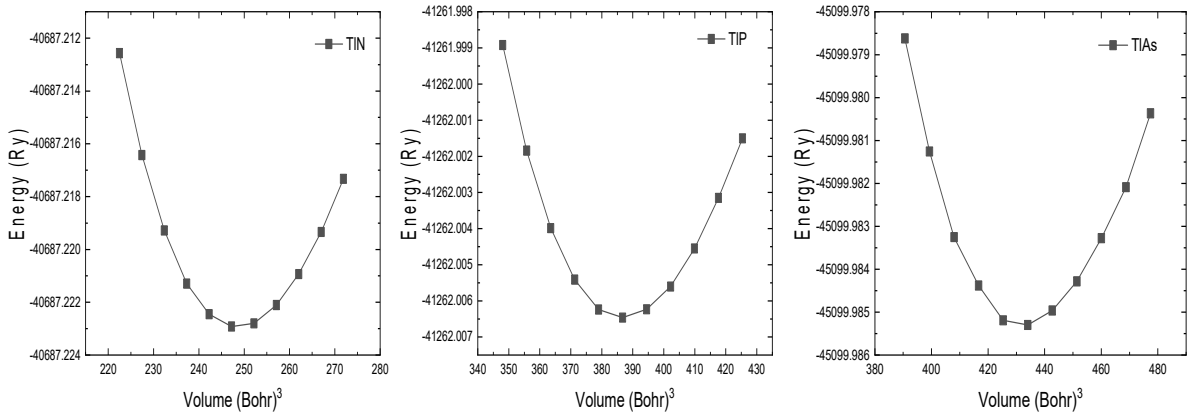

Figure 3. Variation of total energy as a function of atomic volume for TlX compounds in the zinc blend structure

Based on these results, one can conclude that TlX compounds exhibit clear advantages in terms of total energy and thermal stability, making them suitable for optoelectronic applications requiring flexibility and robustness. Conversely, BX compounds—especially BN—are more appropriate for extreme conditions that demand high mechanical performance. This complementary contrast in physical properties paves the way for future hybrid applications that exploit the strengths of both compound families.

Our results are in good agreement with previous theoretical studies, confirming their reliability, however there is no experimental result available for the III-V compounds.

3.2. Electronic parameters

Figures 4 to 7 present the calculated electronic band structures and density of states for BX and TlX compounds in the zinc blende structures. The analysis begins with the boron-based compounds, which exhibit wide band gaps, followed by the thallium-based compounds, whose electronic behavior is influenced by relativistic effects. These results help identify the nature and origin of the band gaps, as will be discussed in the following sections.

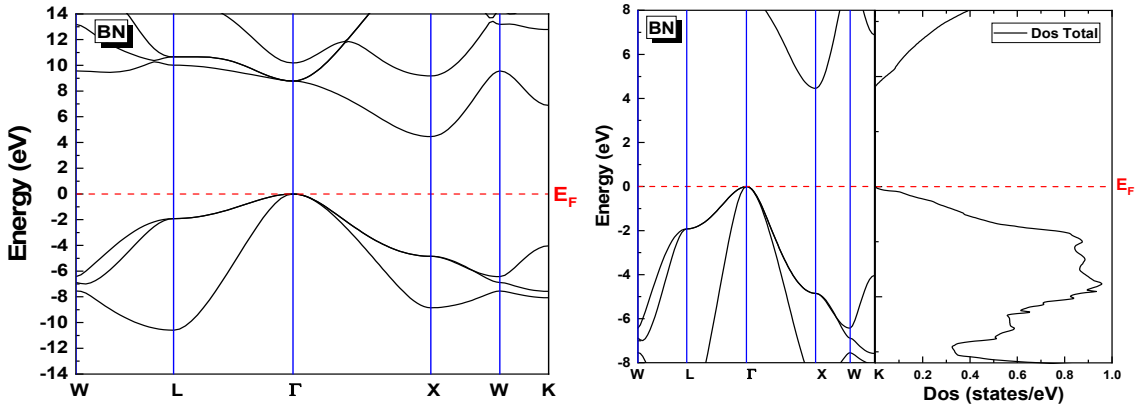

Figure 4. Calculated band structure and total density of states of BX (X=N, P, As) compound

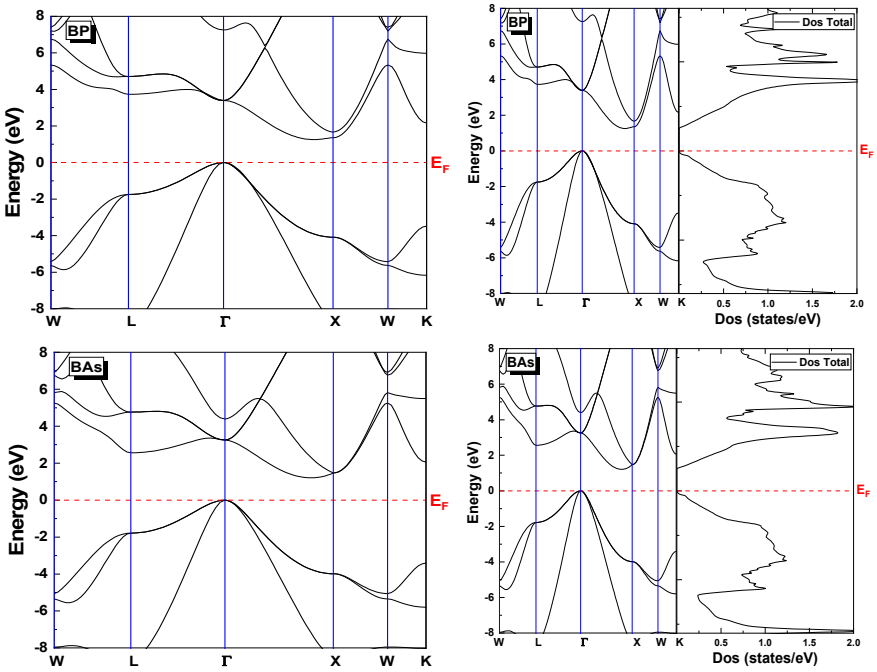

Figure 4. Calculated band structure and total density of states of BX (X=N, P, As) compound (*continued*)

The results are given in Table 3 show that BX (X= N, P, and As) are an indirect gap semiconductor with the minimum of conduction band at Γ, X point.

Table 3. Band gaps of BN, BP, and Bas in the zinc blende structure (all energies are in eV)

compounds	calculations	Other calculations	*Nature of the band gap*
BN	4.4593	4.85 [25], 4.35 [46]	(Γ===X) : *indirect*
BP	1.25317	1.24 [26], 1.14 [27]	(Γ===X) : *indirect*
BAs	1.20819	1.21 [26], 1.23 [30], 1.25 [18], 1.36 [42]	(Γ===X) : *indirect*

The electronic band structure calculations reveal that boron-based compounds BX (X = N, P, As) crystallizing in the zinc blende structure exhibit indirect band gaps. Among these materials, BN possesses the widest band gap, followed by BP and finally BAs with the smallest gap. This decreasing trend in the band gap values is mainly attributed to the increasing atomic number of the group V element. These findings are consistent with recent DFT studies reported in the literature [6. 29]. To gain deeper insights into the electronic structure, the total and partial density of states for BN, BP, and Bas were calculated and illustrated in Figure 5 using the GGA approximation.

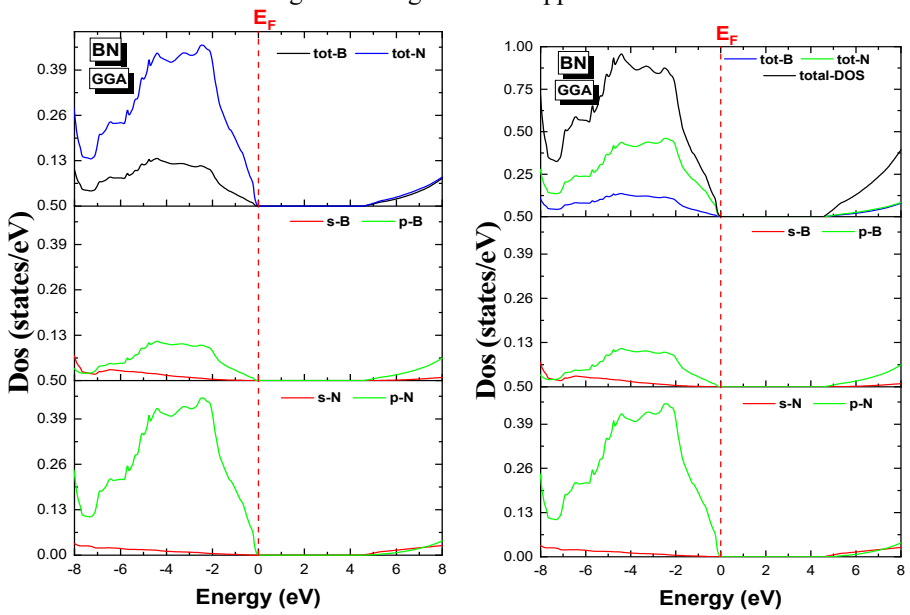

Figure 5. Total and partial densities of states of BX (X=N, P, As). Compound within GGA approximation

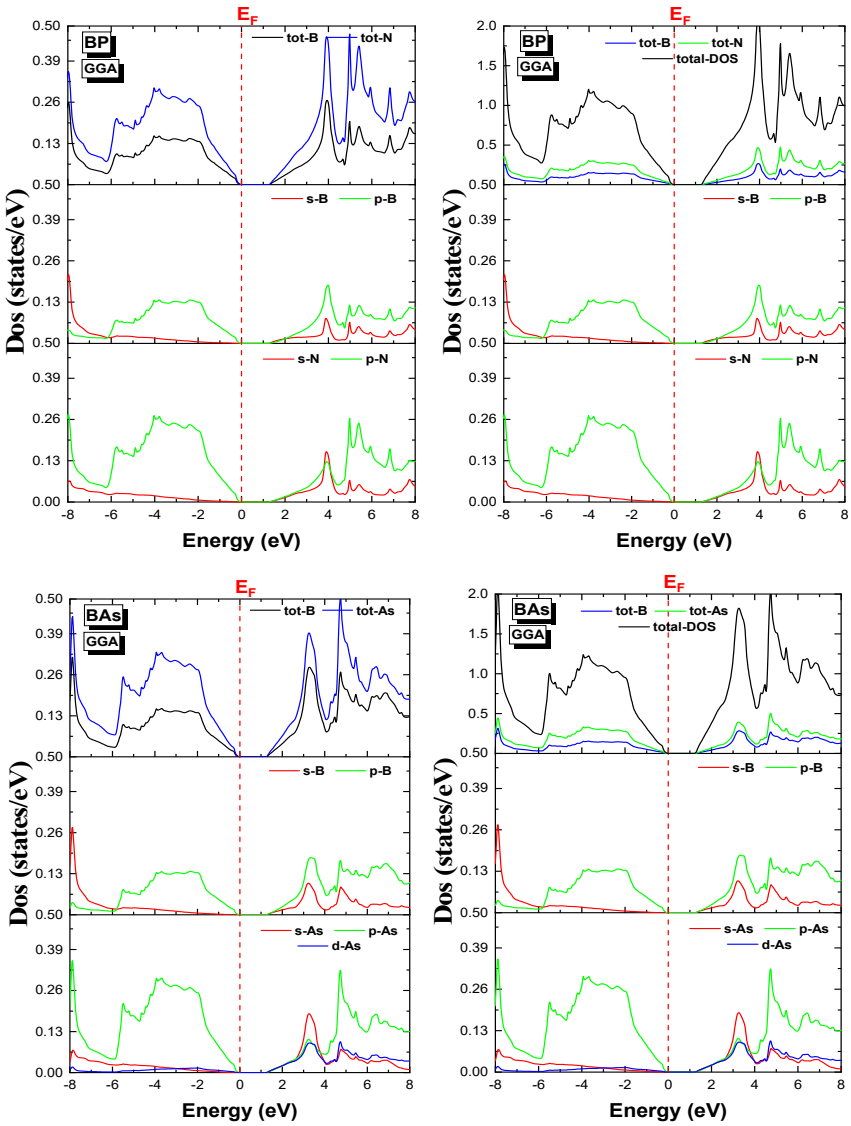

Figure 5. Total and partial densities of states of BX (X=N, P, As). Compound within GGA approximation (*continued*)

Figure 5 presents the total and partial density of states for the BN, BP, and Bas compounds in the Zinc blende structure. For BN, the valence band region, spanning from -8 eV to 0 eV, is strongly dominated by the p orbitals of the nitrogen atom (N-p), with a smaller contribution from the p orbitals of boron (B-p). This indicates a significant ionic character in the B-N bond, driven by the high electronegativity difference between the constituent atoms. In contrast, the conduction band (5-8eV) shows only weak contributions from al orbitals, suggesting a relatively low density of available states for electronic conduction in this energy range.

For BP, both B-p and P-p orbitals contribute significantly within the same valence band range (-8 to 0 eV), while the conduction band (1.25-8 eV) displays distributed contributions from multiple orbitals. This reflects a more covalent and delocalized nature of bonding compared to BN. As for Bas, the valence band is characterized by overlapping contributions from p orbitals of both boron and arsenic (B-p and As-p) within the -8 eV to 0 eV range, whereas the d orbitals of arsenic (As-d) exhibit nearly negligible participation. In the conduction band region (1.2-8eV), the electronic density remains distributed across the same previously mentioned orbitals, indicating similar bonding characteristics to BP but with a different electronic distribution profile.

After completing the analysis of the structural properties of the BX compounds (BN, BP, BAs), we now move on to the study of the TlX compounds (TlN, TlP, TlAs), in order to highlight the fundamental differences between these two families of materials. Unlike the BX compounds, which exhibit typical characteristics of light-element semiconductors, such as small lattice constants and wide band gaps, the structural properties of the TlX compounds clearly reflect the influence of the heavier thallium atom, resulting in noticeably different behavior. These structural differences are expected to have a direct impact on the electronic and optical properties of these materials.

Therefore, it is important to provide a detailed and precise analysis of the TlX compounds in order to clarify how the incorporation of thallium affects the crystal structure and distinguishes them from their boron-based counterparts.

The bands structure of TlX compounds for ZB phase is show in Fig. 6. Electronic structure calculations based on the GGA approximation reveal that the TlN, TlP, and TlAs compounds, crystallizing in the zinc blende (ZB) structure, exhibit a metallic or semi-metallic character, as indicated by the intersection of the Fermi level (EF) with the conduction band. These results confirm the absence of an energy band gap, with a calculated band gap value of 0 eV for all three materials. These findings are consistent with previous theoretical studies, which have also reported a zero-gap behavior in TlX compounds within the same crystal structure, using both GGA and more advanced functional such as mBJ and HSE 06 [3, 30, 31].

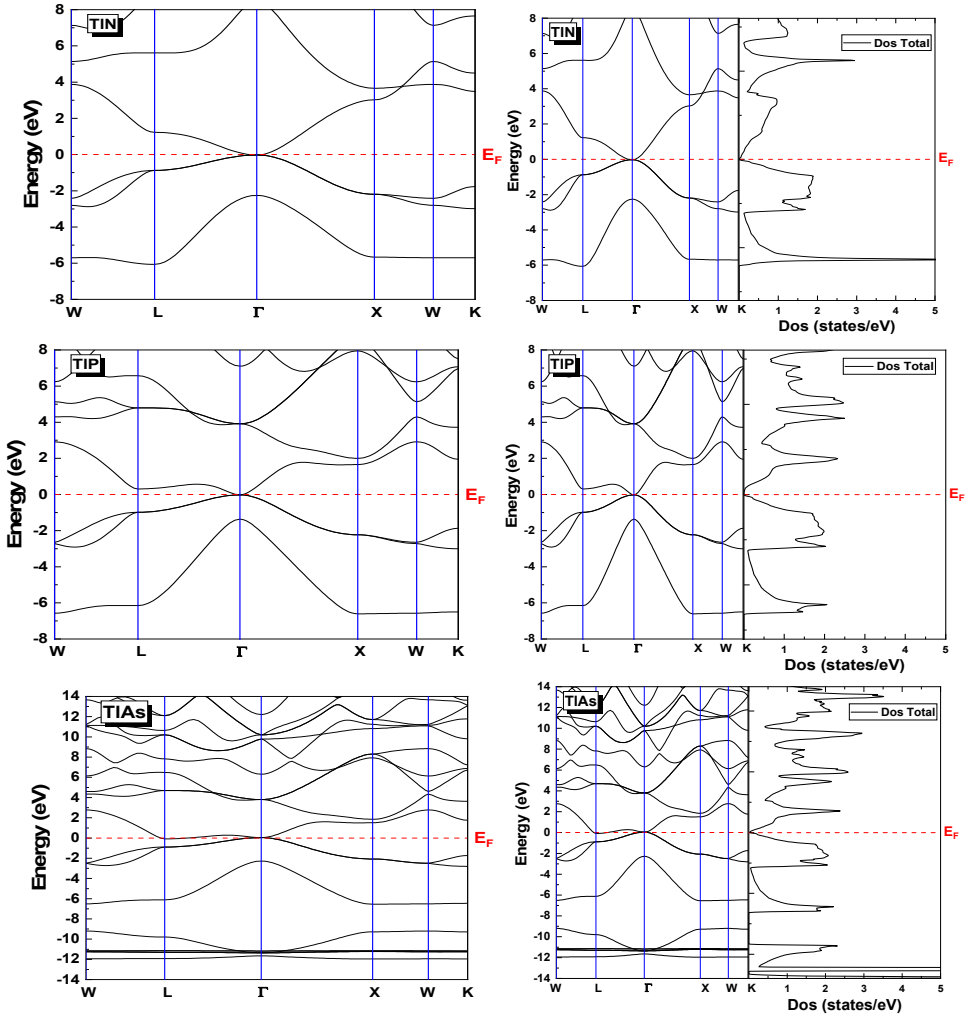

Figure 6. Calculated band structure and total density of states of TlX (X=N, P, As). Compound

To explore the electronic structures in greater detail, the total and partial density of states for TlN, TlP, and TlAs were calculated within the GGA approximation, as illustrated in Figure 7.

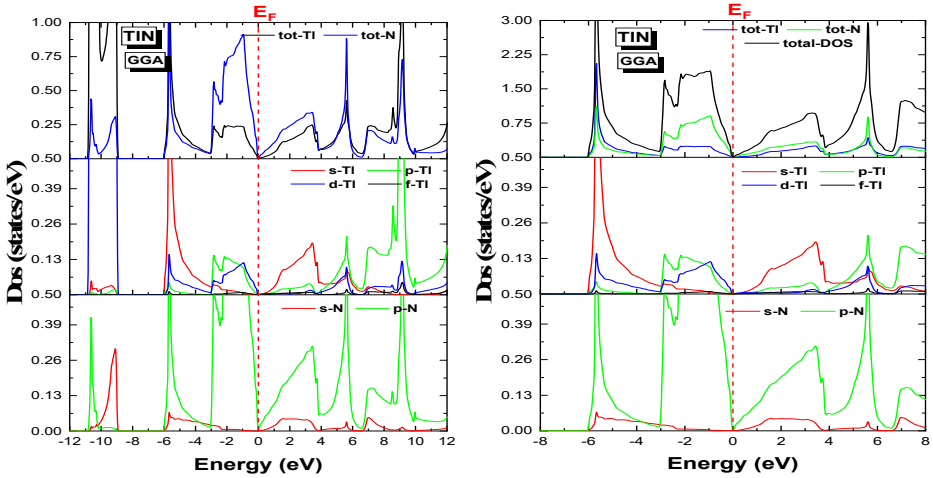

Figure 7. total and partial densities of states of TlX (X=N, P, As). Compound within GGA approximation

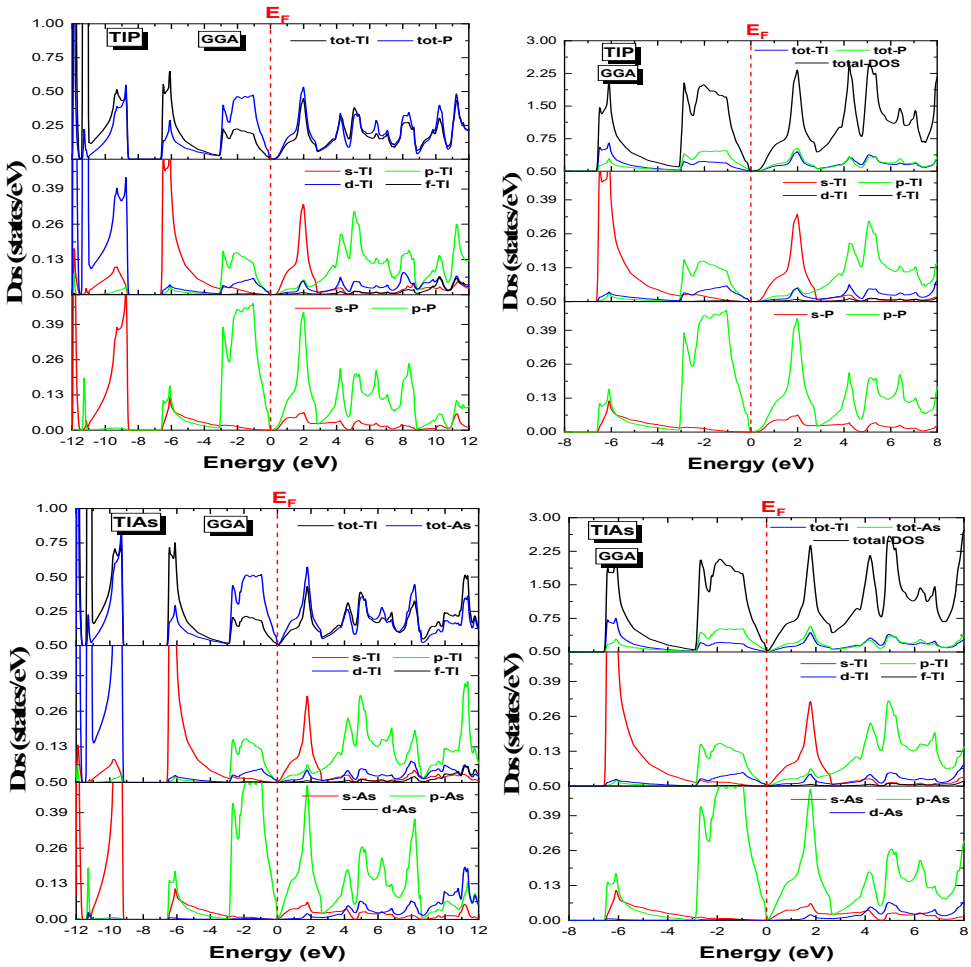

Figure 7. total and partial densities of states of TlX (X=N, P, As). Compound within GGA approximation (*continued*)

A detailed inspection of the partial densty of states for the TlX compounds reveals a clear distinction in the orbital contributions across the valence and conduction bands, which is essential for understanding their electronic behavior and bonding nature.

In the case of thallium nitride, the valence band can be divided into two main regions:

(i) The lower valence band, spanning from approximately -11 to -9 eV is primarily dominated by the Tl-d, N-s, and N-p states. This indicates strong hybridization between thallium and nitrogen deep core levels, reflecting a notable covalent character.

(ii) The upper valence region, from -6 eV to 0 eV, the dominant contributions arise from the Tl-s and N-s orbitals, with a moderate participation of Tl-d and N-s states.

As for the conduction band, starting just above the Fermi level (0 eV) and extending up to 12 eV, it is mainly composed of Tl-p, Tl-s and N-p orbitals. A minor yet noticeable contribution from the Tl-f states is also observed at higher energies, suggesting possible f-character at conduction states in excited conditions.

For TlP the the PDOS profile shows:

(i) A deep valence band segment between-12eV and -9.5 eV,where Tl-d and P-s states dominate, while Tl-s and P-p exhibit weaker contributions.

(ii) In the valence band range from -7eV to 0eV, there is a pronounced mixing for Tl-6p, Tl-s, P-s, and P-p states, with a slight presence of Tl-d this highlights the significant hybridization between thallium and phosphorus s-and p-orbitals near the Fermi level.

In the conduction band, contribution mainly stem from Tl-p, Tl-s, P-s, while Tl-d and Tl-f states appear marginal, indicating limited involvement of deeper core orbitals in the conduction process.

Finally, the PDOS spectrum of thallium arsenide closely resembles that of TlP:

(i) The lower valence band region (-12eV to-9eV) is predominantly characterized by As-s and Tl-d states, marking the interaction between deeper core levels of the two atoms.

(ii) Moving to the upper valence range (-6.5eV to 0eV), significant contributions from Tl-s and As-p are noted, with secondary inputs from Tl-p and As-s

So, in the conduction band (0 to ~8eV), the most pronounced contributions arise from Tl-s, T-p and As-4p, reflecting strong s-p hybridization, essential for the conduction mechanism. Additionally modest involvement of Tl-d, Tl-f, and As-d orbitals is identified at higher energy levels.

The analysis of the electronic band structures alongside the total and partial density of states for TlN, TlP, and TlAs demonstrates that the valence and conduction bands either intersect or come into direct contact at the Fermi level. This particular feature suggests the absence of a real band gap, placing these materials within the category of semi-metallic systems. Such behavior is typically associated with weak orbital hybridization and the influence of relativistic effects linked to the heavy.

So, these differences in the electronic distribution are directly reflected in the physical properties of the compounds. While the BX compounds retain a tunable semiconducting behavior, the TlX compounds appear unsuitable for conventional electronic applications, but they may be exploited in systems with metallic or semi-metallic character.

3.3. Optical parameters

Optical properties play a crucial role in evaluating the potential of materials for electronic and optoelectronic applications, such as detectors and photonic devices. These properties are derived from the energy-dependent dielectric function. In the following, we analyze key optical parameters including reflectivity *R(ω)*, absorption coefficient *α(ω),* energy loss function *L(ω*, and *ε1(ω) and ε2(ω* the real and imaginary parts of the refractive index *n(ω)*. These optical properties were investigated for the studied compounds within the photon energy range of 0 to 14 eV.

The complex dielectric function is used to describe the linear response of a material under an external electromagnetic field. It distinguishes between the contributions of intra-band and inter-band transitions and is represented by its real (ε_1) and imaginary (ε_2) parts [32]. Generally, the $\varepsilon_1(\omega)$ is closely related to the polarization, while $\varepsilon_2(\omega)$ is closely related to the absorption properties [38]:

$$\varepsilon(\omega) = \varepsilon_1(\omega) + i\varepsilon_2(\omega) \tag{3}$$

The imaginary component of the dielectric function at low photon energies is evaluated through electronic structure computations, relying on the joint density of states and the transition matrix elements between filed and empty electronic states. Subsequently, the real part is derived using the Kramers-Kronig transformation [33].

As previously mentioned, this work provides a detailed presentation and analysis of the main optical properties, such as the refractive index and the absorption coefficient, which are determined according to relations (4) and (5), respectively.

$$n(\omega) = \left[\frac{\varepsilon_1(\omega)}{2} + \frac{\sqrt{\varepsilon_1^2(\omega)+\varepsilon_2^2(\omega)}}{2}\right]^{1/2} \tag{4}$$

$$\alpha(\omega) = \frac{4\pi}{\lambda} k(\omega) \tag{5}$$

In these relations, k represents the extinction coefficient, while λ refers to the wavelength of light in vacuum. Further details on the methodology used to calculate these optical properties can be found in the works of Ambrosch-Draxl and Sofo [34, 35, 36].

The calculated Real and Imaginary Parts of the Dielectric Function $\varepsilon_1(\omega)$ and $\varepsilon_2(\omega)$, Refractive Index n(ω), Energy Loss Function L(ω), Reflectivity R(ω), and Absorption Coefficient α(ω) of BX(X=N, P, As) shown in Fig. 8.

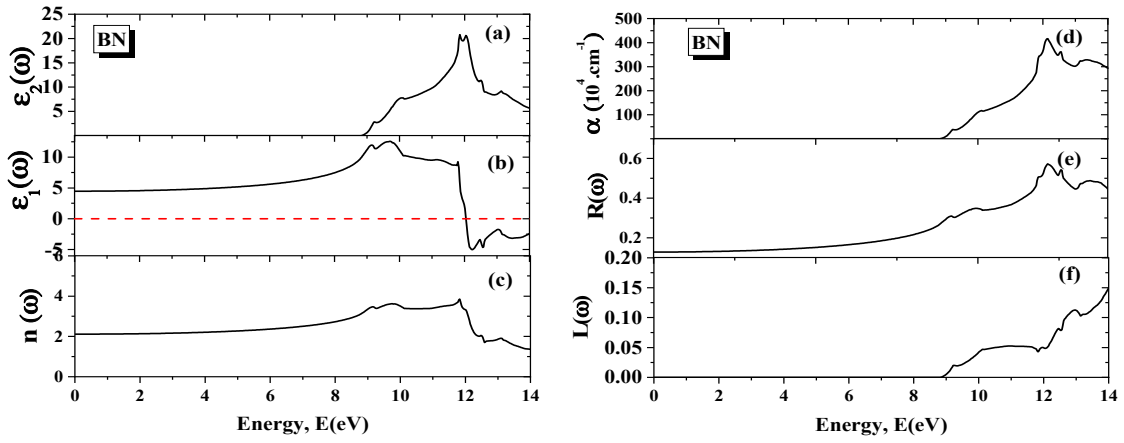

Figure 8. Real and Imaginary Parts of the Dielectric Function $\varepsilon_1(\omega)$ and $\varepsilon_2(\omega)$, Refractive Index n(ω), Energy Loss Function L(ω), Reflectivity R(ω), and Absorption Coefficient α(ω) of BX(X=N, P, As)

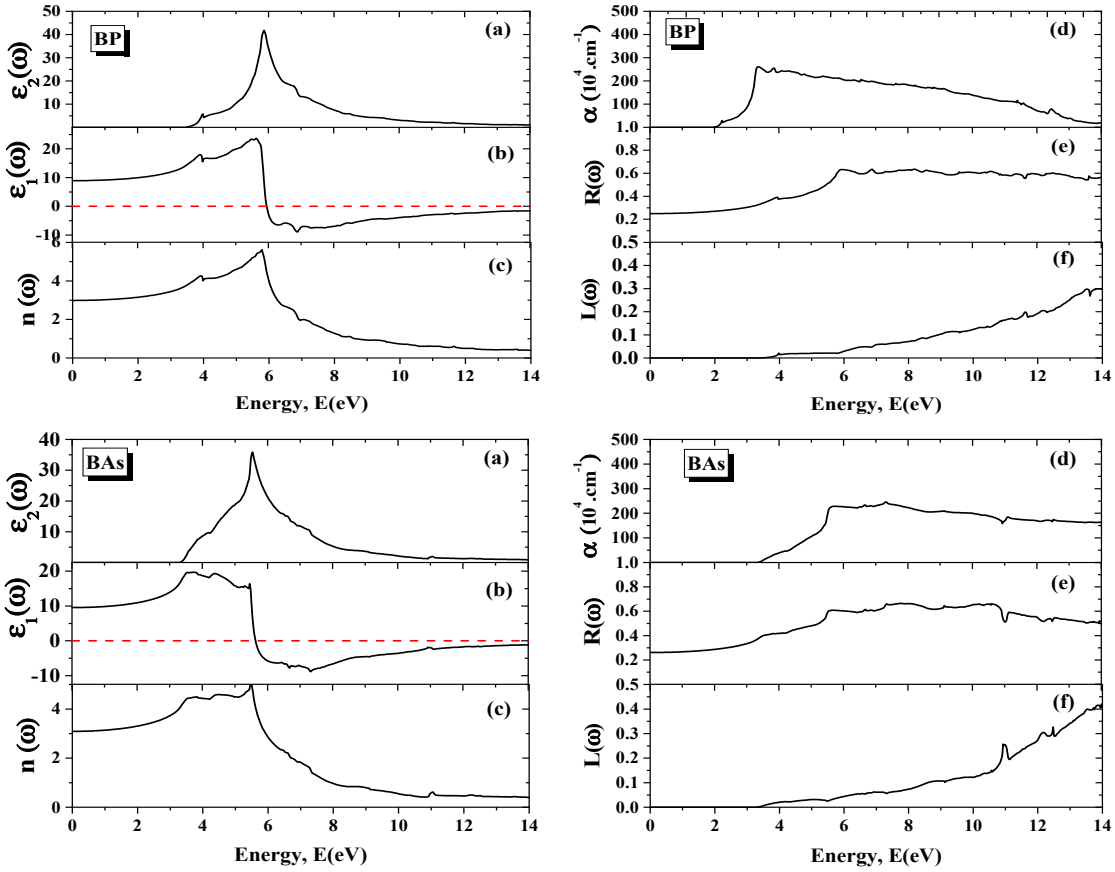

Figure 8. Real and Imaginary Parts of the Dielectric Function ε1(ω) and ε2(ω), Refractive Index n(ω), Energy Loss Function L(ω), Reflectivity R(ω), and Absorption Coefficient α(ω) of BX(X=N, P, As) (*continued*)

Imaginary Part ε2(ω): For BN compound, it is observed that the absorption starts in the ultraviolet region, around 9 eV, which clearly indicates the presence of a wide energy gap. Moreover, the low values of the imaginary part of the dielectric function (ε2) up to this energy confirm the transparency of the material in the infrared, visible, and near-ultraviolet ranges. Beyond this point, ε2 gradually increases, reaching its maximum around 12 eV, reflecting sharp and intense electronic transitions in the deep ultraviolet region. These results are in good agreement with the work reported by Artús et al. [45].

For both BP and BAs compounds, it is observed that the onset of optical absorption starts at an energy value of approximately 3.5 eV for each, indicating that their energy gaps are smaller compared to BN. Moreover, two prominent absorption peaks are recorded for both compounds within the energy range of 5 to 6 eV, with the maximum absorption intensity reaching around 40 for BP and about 35 for BAs. Beyond these peaks, a gradual decrease in absorption is observed until it becomes almost negligible in the deep ultraviolet region for both compounds.

Real Part ε1 (ω): For the BN compound in the energy range between 0 and 6 eV (from the infrared to the near-ultraviolet region), the real part ε1 remains approximately constant. Subsequently, this value increases gradually, reaching a maximum of about 12.5 at energy of approximately 10 eV, which corresponds to the deep ultraviolet region. Beyond this point, ε1 decreases significantly and becomes negative at higher photon energies, indicating the occurrence of plasmonic response in this energy range. For the BP and BAs compounds At 0 eV, the imaginary part ε2 is around 9 for BP and approximately 10 for BAs. These values remain nearly constant in both the infrared and visible regions. As the photon energy increases, ε2 starts to rise gradually until two pronounced peaks appear in the near-ultraviolet region:

(i) A pronounced peak around 25 is observed for BP within the energy range of 5-6 eV.

(ii) Another peak around 20 for BAs, located in the energy range between 3 and 4 eV.

Refractive Index n(ω): For BN, the static refractive index is n(0) = 2.1. This value remains almost constant up to (≈ 9 eV), beyond which it increases, reaching its maximum peak at around 12 eV. After this point, the refractive index decreases rapidly. In the case of BP, the static refractive index is n(0) = 3. This value remains nearly unchanged in the low-energy region up to about 4 eV, where the first peak appears with a refractive index of 4. Subsequently, the highest peak emerges at around 5.7 eV with a maximum value of n = 5.5, followed by a continuous decrease. For BAs, the static refractive index is n (0) = 3.1. A distinct peak appears at around 5.5 eV. These results are in good agreement with the work reported by Artús et al. [45]

Absorption Coefficient α(ω): The curves illustrating the variation of the absorption coefficient as a function of photon energy reveal the following behavior: For BN, no absorption is observed up to approximately 9 eV in the ultraviolet (UV) region. Beyond this energy, the absorption gradually increases, reaching its maximum peak around 12 eV in the deep UV region. For BP, the absorption remains negligible up to about 2 eV. It then increases progressively, reaching a maximum value of approximately 250 at around 3.2 eV, followed by a decrease.

For BAs, the absorption is absent in both the infrared and visible regions. It starts to increase at higher photon energies, reaching a maximum value of approximately 250, and then gradually decreases thereafter.

Reflectivity R(ω): The optical reflectivity of the compounds BN, BP, and BAs exhibits distinct behaviors for each material. For BN, at the zero-energy limit, the reflectivity is approximately 0.06% in the infrared region, and it gradually increases with photon energy, reaching about 0.5% in the deep ultraviolet region. For BP, the reflectivity at zero energy is R(0) = 0.25%. Nearly equal peaks of about 0.65% are observed within the energy range between 6 and 14 eV.

For BAs, the zero-energy reflectivity is approximately R(0) = 0.28%. It gradually increases beyond 5.5 eV, reaching values between 0.5% and 0.7%. The absence of absorption in the infrared region, along with the low reflectivity values, highlights the potential of these materials for use as cold, anti-reflective coatings in optical fiber technologies.

Energy Loss Function L(ω): Based on the analysis of the electron energy loss function (EELF) data, it is observed that the maximum peak for BN appears at approximately 14 eV. In contrast, for the compounds BP and BAs, the main peaks of the energy loss function are located within the energy range of 13.5 to 14 eV, indicating a similar optical behavior in this energy interval, which is typically associated with the plasmon excitation energies of these materials.

It is worth mentioning that some of the obtained results are in good agreement with several recent studies, which reinforces the validity of the reliability of the achieved findings [39, 40, 41, 42]. In this section, we will analyze the optical calculation results of thallium compounds So that the calculated Real and Imaginary Parts of the Dielectric Function $\varepsilon_1(\omega)$ and $\varepsilon_2(\omega)$, Refractive Index n(ω), Energy Loss Function L(ω), Reflectivity R(ω), and Absorption Coefficient α(ω) of TX(X=N, P, As) shown in Figure. 9.

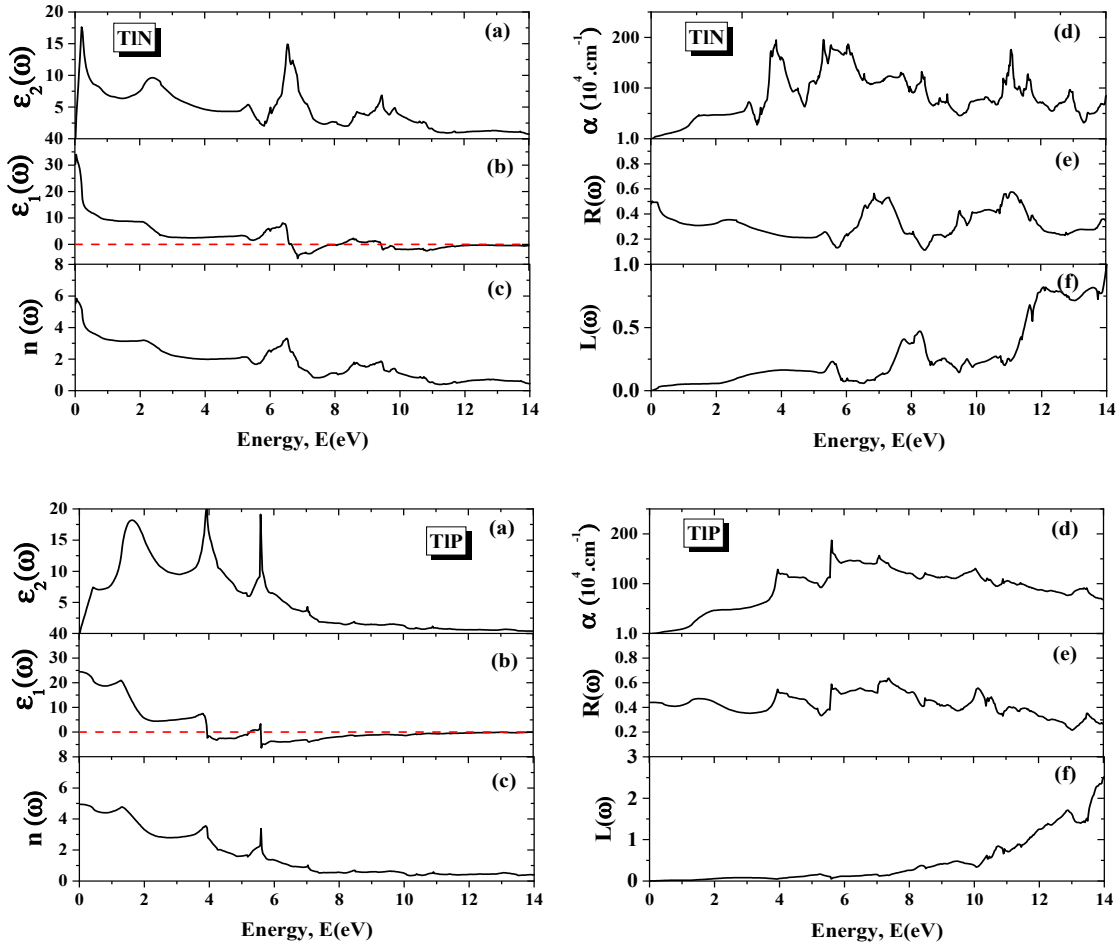

Figure 9. Real and Imaginary Parts of the Dielectric Function $\varepsilon_1(\omega)$ and $\varepsilon_2(\omega)$, Refractive Index n(ω), Energy Loss Function L(ω), Reflectivity R(ω), and Absorption Coefficient α(ω) of TX(X=N, P, As) and TlX(X=N, P, As)

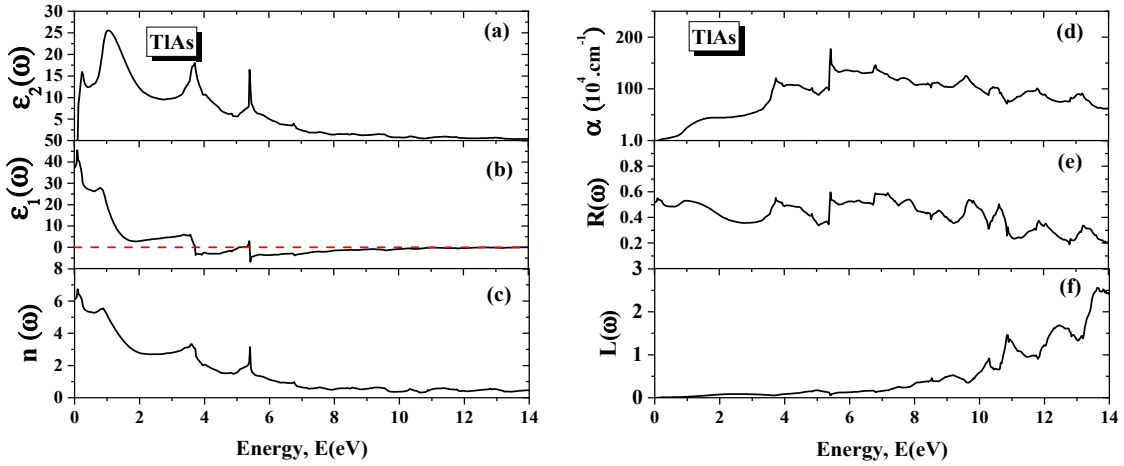

Figure 9. Real and Imaginary Parts of the Dielectric Function $\varepsilon_1(\omega)$ and $\varepsilon_2(\omega)$, Refractive Index $n(\omega)$, Energy Loss Function $L(\omega)$, Reflectivity $R(\omega)$, and Absorption Coefficient $\alpha(\omega)$ of TX(X=N, P, As) and TlX(X=N, P, As) (*continued*)

Imaginary Part $\varepsilon_2(\omega)$: The thallium compounds exhibit remarkable optical activity in the low-energy range. For TlN, distinct peaks are observed up to approximately 10 eV, with the most intense peak occurring below 1 eV, which corresponds to the infrared region. As for TlP and TlAs, noticeable peaks appear up to around 6 eV, after which the intensity gradually decreases.

Real Part $\varepsilon_1(\omega)$: The real part of the dielectric function $\varepsilon 1(\omega)$ is considered a key factor in understanding the optical behavior of this class of compounds, as it reflects the material's ability to polarize under the influence of external electromagnetic fields.

According to the obtained results, the highest values of $\varepsilon 1$ are recorded at 0 eV, which corresponds to the infrared region, indicating a strong capacity of these materials to store electric energy in this energy range. Among the studied compounds, the highest static dielectric constant was observed for TlAs, with $\varepsilon_1(0) = 45$, followed by TlN with a value of approximately $\varepsilon_1(0) = 35$, and finally TlP with $\varepsilon_1(0) = 25$. These results highlight the differences in polarization ability among the compounds, where TlAs exhibits a stronger polarizability compared to TlN and TlP, which is reflected in their distinct electromagnetic responses at low frequencies

Index n(ω): In this study, the refractive index at zero photon energy is extracted from the optical spectra as follows: $n(0) = 6.7$ for TlN, $n(0) = 5$ for TlAs, and $n(0) = 5$ for TlP. These values highlight the relatively high refractive indices of the thallium-based compounds in comparison with boron-based compounds, especially in the low-energy region. With increasing photon energy, the refractive index decreases progressively to reach values as low as 0.5 beyond 10 eV, indicating a weak refractive response at high energies.4. These results are in good agreement with the findings reported in 2023, which confirmed that materials with small or negligible band gaps generally exhibit high refractive index values at low photon energies, followed by a gradual decrease as the photon energy increases, according to the Wemple–DiDomenico model [44].

Absorption Coefficient α(ω): The optical absorption of the studied compounds starts within the infrared region and gradually increases, exhibiting pronounced peaks in the energy range between 3.5 and 6.5 eV. Additionally, for TlN, a distinct absorption peak appears around 13 eV, indicating active electronic transitions within these energy regions. For the compounds TlP and TlAs, two sharp peaks are observed near 6 eV for each, followed by a gradual decrease in the absorption coefficient. This behavior reflects a reduction in the density of electronic transitions in this energy range [43].

Reflectivity R(ω): The initial reflectivity values for the three compounds are approximately similar, with about 0.5 for TlN, 0.45 for TlP, and 0.51 for TlAs at zero photon energy. For TlN, two distinct reflectivity peaks are observed: the first located around 7 eV, and the second between 10 and 12 eV. In contrast, TlP and TlAs exhibit less pronounced and more gradually diminishing peaks as the photon energy increases. Notably, unlike TlP and TlAs, the reflectivity of TlN decreases between 11 and 12.5 eV, but shows a slight increase beyond this range.

Energy Loss Function L(ω): The energy loss function exhibits a low initial peak for all the compounds (TlN, TlP, and TlAs), followed by a clear increase starting from around 8 eV. A prominent and well-defined main peak is identified for each compound at approximately 14 eV, indicating strong energy loss behavior in this energy region.

4. CONCLUSIONS

In this study, the structural, electronic, and optical properties of thallium-based compounds TlX (X = N, P, As) and boron-based compounds BX (X = N, P, As) in the zinc-blende structure were systematically investigated using density functional theory (DFT) within the GGA approximation. The obtained results reveal that boron compounds exhibit a typical semiconductor behavior with well-defined energy gaps, while thallium compounds exhibit a nearly metallic

behavior with a vanishing energy gap. From the optical perspective, all compounds show a decreasing trend in the refractive index as photon energy increases, starting from relatively high values at low energies, which indicates a weak optical response at high photon energies. Furthermore, the analyses of the absorption spectra and dielectric functions highlighted the presence of significant electronic transitions at specific energy ranges for each compound, reflecting the density of available electronic states. These findings clearly demonstrate the distinct electronic and optical behaviors between thallium-based and boron-based compounds, underscoring their potential relevance for advanced electronic and optoelectronic applications. Moreover, the observed trends are largely consistent with recent theoretical studies cited throughout this work.

Acknowledgments

I would like to express my sincere gratitude to my supervisor, Professor Lachebi Abdelhadi, for his continuous support, valuable guidance, and insightful remarks that significantly contributed to the successful completion of this work. I would also like to extend my heartfelt thanks to my colleague, El Aid Abdelali, for his constant encouragement and fruitful collaboration throughout the preparation of this research.

ORCID

Abed Zoulikha, https://orcid.org/0009-0007-4824-1099; **Abdelali Laid**, https://orcid.org/0009-0009-9173-3835

REFERENCES

[1] A.M, Satawara, G.A. Shaikh, S.K. Gupta, and P.N. Gajjar, "Structural, electronic and optical properties of hexagonal boron-nitride (h-BN) monolayer: An Ab-initio study," Material Today: Proceedings, **47**(10), 529-532 (2020). https://doi.org/10.1016/j.matpr.2020.10.589

[2] D. Allali, B. Abdelmajid, S.E. Saber, D. Bahri, F. Zerarga, R. Amari, M. Radjai, *et al*. "Afirst-principles investigation on the structural, electronic and optical characteristics of tetragonal compounds XAgO (X = Li, Na, K, Rb)," Computational Condensed Matter. **38**, e00876 (2024). https://doi.org/10.1016/j.cocom.2023.e00876

[3] N. Saidi-Houat, A. Zaoui, and M. Ferhat, "Structural Stability of Thallium–V Compounds," Journal of Physics: Condensed Matter, **19**(10), 106221 (2007). https://doi.org/10.1088/0953-8984/19/10/106221

[4] C. Ambrosch-Draxi, and J.O. Sofo, "Linear optical properties of solids within the full- potential linearized augmented plane wave method," Computer Physics Communications, **175**, 1-14 (2006). https://doi.org/10.1016/j.cpc.2006.03.005

[5] J.P. Perdew, K. Burke, and M. Ernzerhof, "Generalized Gradient Approximation Made Simple," Physical Review Letters, **77**, 3865–3868 (1996). https://doi.org/10.1103/PhysRevLett.77.3865

[6] Y. Megdoud, Y. Benkrima, L. Tairi, R. Meneceur, S. Ghemid, and H. Meradji, Functional materials, **31**(2), 232-251 (2024). https://doi.org/10.15407/fm31.02.232

[7] F.D. Murnaghan, "The compressibility of media under extreme pressures," Proceedings of the national Academy of Sciences, **30**(9), 244-247 (1944). https://doi.org/10.1073/pnas.30.9.244

[8] P. Blaha, K. Schwarz, G.K.H. Madsen, D. Kvasnicka, and J. Luitz, *WIEN2K: An Augmented Plane Wave plus Local Orbitals Program for Calculating Crystal Properties,* (J. Techniche Universtät Wien,Wien. Austria, 2001).

[9] Alleg Abdelakader, Benamara Ahmed, Moulay Noureddine, Berrahal Mokhtar, Zoukel Abdelhalim; Mansour Omar, Bensaid Djillali, Azzaz Yahia, Y. Al-Douri, Solid State Communications 380, 115435 (2024). https://doi.org/10.1016/j.ssc.2024.115435

[10] H.J. Monkhorst, and J.D. Pack, "Special points for Brillouin-zone integrations," Phys. Rev. B, **13**, 5188-5192 (1976). https://doi.org/10.1103/PhysRevB.13.5188

[11] H. Allaf, M. Radjai, D. Allali, A. Bouhemadou, S.S. Essaoud, S.B. Omran, R. Khenata, and Y. Al-Douri, "Ab initio predictions of pressure-dependent structural, elastic, and thermodynamic properties of $CaLiX_3$ (X = Cl, Br, and I) halide perovskites," Computational Condensed Matter, **37**, E00850 (2023). https://doi.org/10.1016/j.cocom.2023.e00850

[12] D. Allali, R. Amari, A. Bouhemadou, A. Boukhari, B. Deghfel, S.S. Essaoud, S. Bin-Omran, *et al*. "*Ab initio* investigation of structural, elastic, and thermodynamic characteristics of tetragonal XAgO compounds (X = Li, Na, K, Rb)," Physica Scripta, **98**, 115905 (2023). https://doi.org/10.1088/1402-4896/acfbfe

[13] J.I. Al-Hawarin, A.-A. Abu-Yamin, Abd Al-Aziz A. Abu-Saleh, I.A.M. Saraireh, M.H. Almatarneh, M. Hasan, O.M. Atrooz, *et al*. "Synthesis, Characterization, and DFT Calculations of a New Sulfamethoxazole Schiff Base and Its Metal Complexes," Materials, **16**(14), 5160 (2023). https://doi.org/10.1088/1402-4896/acfbf

[14] R. Samia, A. Yahia, B. Ahmed, B. Mokhtar, M. Noureddine, L. Mohamed, B. Djillali, *et al*. "Electronic, elastic and piezoelectric properties calculations of perovskites materials type BiXO3(X = Al, Sc): DFT and DFPT investigations," Chemical Physics, **573**, 111998 (2023). https://doi.org/10.1016/j.chemphys.2023.111998

[15] M. Farzan, S.M. Elahi, H. Salehi, and M.R. Abolhassani, "A Comparison of the~Structural, Electronic, Optical and Elastic Properties of Wurtzite, Zinc-Blende and Rock Salt TlN: A DFTStudy," Acta Phys. Pol. A, **130**(3), 758–768 (2016). https://doi.org/10.12693/APhysPolA.130.758

[16] A. El Hassasna, and A. Bechiri, "Electronic and Elastic Properties of TlX (X = N, P, As and Sb) in Zinc-Blende Structure," Solid State Phenom. **297**, 82–94 (2019). https://doi.org/10.4028/www.scientific.net/SSP.297.82

[17] K. Bencherif, A. Yakoubi, and H. Mebtouche, "Structural and Electronic Properties of the BN, BP and BAs in the Different Phases of Zinc-Blende, NaCl and CsCl," Acta Phys. Pol. A, **131**(1), 209–212 (2017). https://doi.org/10.12693/aphyspola.131.209

[18] R.M. Wentzcovitch, M.L. Cohen, and P.K. Lam, "Theoretical study of BN, BP, and BAs at high pressures," Phys. Rev. B, **36**(11), 6058 (1987). https://doi.org/10.1103/PhysRevB.36.6058

[19] M. Van Shilfgaarde, A.-B. Chen, S.S.A. Krishnamurthy and A. Sher, "InTlP – a proposed infrared detector material," Appl. Phys. Lett. **65**, 2714–2716 (1994). https://doi.org/10.1063/1.112567

[20] N. Saidi-Houat, A. Zaoui, and M. Ferhat, "Ab initio study of the fundamental properties of novel III-V nitride Alloys $Ga_{1-x}Tl_xN$," Materials Science and Engineering B, **162**, 26-31 (2009). https://doi.org/10.1016/j.mseb.2009.01.031

[21] H.M. Mazouz, A. Belabbes, A. Zaoui, and M. Ferhat, "First-principles study of lattice dynamics in thallium-V compounds," Superlatices and Microstructures, **48**, 560-5568 (2010). https://dx.doi.org/10.1016/j.spmi.2010.09.012

[22] B.B. Bouiadjra, N. Mehnane, and N. Oukli, "First principles calculation of structural, electronic and optical properties of (001) and (110) growth axis (InN)/(GaN)n superlattices," Revista Mexicana de Fisica, **67**(1), 7-17 (2021). https://doi.org/10.31349/RevMexFis.67.7

[23] R. Riane, Z. Boussahla, S.F. Matar, and A. Zaoui, "Structural and Electronic Properties of Zinc Blende-type Nitrides $B_xAl_{1-x}N$," Z. Naturforsch. **63**(9), 1069-1076 (2008). https://doi.org/10.1515/znb-2008-0909

[24] S. Adachi, *Properties of Group IV, III–V and II–VI Semiconductors*, (John Wiley & Sons, 2005). https://doi.org/10.1002/0470090340

[25] A. Said, M. Debbichi, and M. Said, "Theoretical study of electronic and optical properties of BN, GaN and $B_xGa_{1-x}N$ in zinc blende and wurtzite structures," Optik, **127**(20), 9212–9221 (2016). https://doi.org/10.1016/j.ijleo.2016.06.103

[26] H. Meradji, S. Drablia, S. Ghemid, H. Belkhir, B. Bouhafs, and A. Tadjer, "First-principles elastic constants and electronic structure of BP, BAs, and BSb," Phys. Status Solidi B, **241**(13), 2881–2885 (2004). https://doi.org/10.1002/pssb.200302064

[27] P. Rodriguez-Hernandez, M. Gonzalez-Diaz, and A. Munoz, Phys. Rev. B, **51**, 14705 (1995). https://doi.org/10.1103/physrevb.51.14705

[28] A. Zaoui, M. Ferhat, B. Khelifa, J.P. Dufour, and H. Aourag, "Correlation between the Ionicity Character and the Charge Density in Semiconductors," Phys. Stat. Sol. (b), **185**, 163-169 (1994). https://doi.org/10.1002/pssb.2221850112

[29] H. Belghoul, M. Oukli, F. Moulay, K. Ghlam, and H. Abid, "First-principles calculations to investigate structural, electronic and optical properties of BN by inserting an ultrathin XY(X = B, Al and Y= Bi, P, N) layer to form short-period (XY)1/(BN)1 superlattice," Optoelectronics and Advanced Materials," **18**(7-8), 363-382 (2024).

[30] S.E. Gulebaglan, E.K. Dogan, M. Aycibin, M.N. Secuk, B. Erdinc, and H. Akkus. "Structural and electronic properties of zincblende phase of $Tl_xGa_{1-x}As_yP_{1-y}$ quaternary alloys: First-principles study," Cent. Eur. J. Phys. **11**(12), 1680-1685 (2013). https://doi.org/10.2478/s11534-013-0314-1

[31] S.Q. Wang. H.Q. Ye, "," Phys. Rev. B, **66**, 235111 (2002). https://doi.org/10.1103/PhysRevB.66.235111

[32] Y. Al-Douri, B. Merabet, H. Abid, and R. Khenata, "First-principles calculations to investigate optical properties of ByAlxIn1−x−yN alloys for optoelectronic devices," Superlattice and Microstructures, **51**, 404-411 (2012). https://doi.org/10.1016/j.spmi.2012.01.004

[33] S. Alnujaim, A. Bouhemadou, M. Chegaar, A. Guechi, S. Bin-Omran, R. Khenata, Y. Al-douri, W. Yang. and H. Lu, "Density functional theory screening of some fundamental physical properties of Cs2InSbCl6 and Cs2InBiCl6 double perovskites," The European Physical Journal B, **95**, 114 (2022). https://doi.org/10.1140/epjb/s10051-022-00381-2

[34] M. Merabet, S. Benalia, L. Djoudi, O. Cheref, N. Bettahar, D. Rached, R. Belacel, Chinese Journal of Physics 60, 462 (2019). https://doi.org/10.1016/j.cjph.2019.05.026.

[35] C. Ambrosch-Draxl, and J.O. Sofo, "Linear optical properties of solids within the full-potential linearized augmented planewave method," Computer Physics Communications, **175**, 1-14 (2006). https://doi.org/10.1016/j.cpc.2006.03.005

[36] D.P. Rai, Sandeep, A. Shankar, A.P. Sakhya, T.P. Sinba, P. Grima-Gallardo, H. Cabrera, R. Khenata, *et al*. "Electronic, optical and thermoelectric properties of bulk and surface (001) CuInTe2: A first principles study," Journal of Alloys and Compounds, **699**, 1003-1011 (2017). https://doi.org/10.1016/j.jallcom.2016.12.443

[37] A. El Hassasna, and A. Bechiri, "Electronic and Elastic Properties of TlX (X= N, P, As and Sb) in zinc-Blende Structure," Solid State Phenomena, **297**, 82-94 (2019). https://doi.org/10.4028/www.scientific.net/SSP.297.82

[38] S. Ding, H. Zhang, R. Dou, W. Liu, D. Sun, and Q. Zhang, "Theoretical and Experimental studies of electronic, optical and luminescent properties for Tl-based garnet materials," J. Solid State Chem. **263**, 123-130 (2018). https://doi.org/10.1016/J.JSSC.2018.04.028

[39] B. Song, *et al*. "Optical Properties of cubic boron arsenide," Applied Physics Letters, **116**, 141903 (2020). https://doi.org/10.1063/5.0004666

[40] X. Huang, Q. Cao, M. Wan, and H.-Z. Song, "Electronic and optical properties of BP, InSe mono layer and BP/InSe Heterojunction with promising photo electronic performance," Materials, **15**, 6214 (2022). https://doi.org/10.3390/ma15186214

[41] M.M. Nobahari, "Electro-optical properties of strained mono layer boron phosphide," Scientific-Reports, **13**, 9849 (2023). https://doi.org/10.1038/s41598-023-37099-9

[42] E. da Silva Barboz, A.A. Dias, L. Graco, S.S. Carara, D. Da Costa, and T.A.S. Pereira. "Electronic, excitonic, and optical properties of zinc blende boron arsenide tuned by hydrostatic pressure," ACS Omega, **9**, 47710-47718 (2024). https://doi.org/10.1021/ACSOMEGA.4C07598

[43] C. Zhang, S. Mahadevan; J. Yuan, J.K. Wai, H.Y. Gao, W. Liu, H. Zhong, *et al*. "Unraveling Urbach Tail Effects in High-Performance Organic Photovoltaics: Dynamic vs Static Disorder," ACS Energy Lett. **7**(6), 1971-1979 (2022). https://doi.org/10.1021/acsenergylett.2c00816

[44] A. Lamichhane, "Energy–Gap–Refractive Index Relations in Semiconductors—Using Wemple–DiDomenico Model to Unify Moss, Ravindra, and Herve–Vandamme Relationships," Solids, **4**(4), 316–326 (2023). https://doi.org/10.3390/solids4040020

[45] L. Artús. M. Feneberg, C. Attaccalite, J.H. Edgar, J. Li, R. Goldhahn, and R. Cuscó, "Ellipsometry Study of Hexagonal Boron Nitride Using Synchrotron Radiation: Transparency Window in the Far-UVC," Adv. Photonics Res. **2**(4), 2000101 (2021). https://doi.org/10.1002/adpr.202000101

[46] A. Zaoui, and F. El Haj Hassan, "Full potential linearized augmented plane wave calculations of structural and electronic properties of BN, BP, BAs and BSb," J. Phys. Condens. Matter, **13**, 253 (2001). https://doi.org/10.1088/0953-8984/13/2/303

ДОСЛІДЖЕННЯ СПОЛУК TlX ТА BX (X= N, P, As) НА ОСНОВІ DFT: ПОРІВНЯЛЬНИЙ ОГЛЯД СТРУКТУРНОЇ, ЕЛЕКТРОННОЇ ТА ОПТИЧНОЇ ПОВЕДІНКИ

Абед Зуліха, Лачабі Абдельхаді, Абделалі Лаїд

Лабораторія прикладних матеріалів, дослідницький центр, Університет Сіді-Бель-Аббес, 22000, Алжир

У цій роботі представлено детальне теоретичне дослідження структурних, електронних та оптичних властивостей сполук на основі талію (TlX) та бору (BX), де X = N, P, As, у кристалічній структурі цинкової суміші. Розрахунки з перших принципів були виконані з використанням теорії функціоналу густини (DFT) в узагальненому градієнтному наближенні (GGA). Отримані результати показують, що сполуки на основі Tl демонструють нижчі загальні енергії порівняно зі сполуками BX, що вказує на вищу структурну стабільність. З точки зору електронної поведінки, сполуки BX зберігають свою напівпровідникову природу. На відміну від цього, сполуки TlX демонструють металеві або майже металеві характеристики через відсутність енергетичної щілини на рівні Фермі. Крім того, оптичні дослідження показують, що сполуки TlX мають вищі статичні показники заломлення та сильніші характеристики поглинання в області низьких енергій. Ці результати підкреслюють потенціал сполук на основі Tl для майбутнього застосування в оптоелектронних та фотонних пристроях. Загалом, це порівняльне дослідження надає цінні знання для розробки передових матеріалів для електронних та енергетичних технологій.

Ключові слова: *сполуки талію; сполуки бору; розрахунки з перших принципів; теорія функціоналу густини (DFT); електронні властивості; зонна структура; напівпровідники; TlX; BX*